Close Integration of a UHF-RFID Transponder Into a Limb Prosthesis for Tracking and Sensing

Rossella Lodato and Gaetano Marrocco

***Abstract*— The technology of structural radio systems that is well assessed in the avionic and naval communications is here applied to obtain antenna functionality out of a limb prosthesis with minimal changes to the device, in specific, an orthopedic nail. A microchip transponder based on the ultrahigh frequency-radio-frequency identification (RFID) communication standard is connected to the nail by means of a central notch forming a towel-bar-like antenna. The resulting device, called prosthetic structural tag, is such to preserve the mechanical continuity of the original nail, but it is also capable of energy harvesting and RFID. The electrical and geometrical control parameters for impedance tuning were identified using computer simulation and laboratory tests. The radiation performance is mostly dependent on the geometry of the notch, while it is rather unaffected by the length of the nail, so that the proposed layout may also be applied to different kinds of prosthesis. The experimented read distance at 870–960 MHz was more than 35-cm far from the limb surface. The augmented smart prosthesis is, hence, suitable to be monitored using an external non-contacting antenna for application to tracking and, in the near future, to monitor the prosthesis health status.**

***Index Terms*— Implantable antenna, sensor, radio frequency identification (RFID), temperature.**

I. Introduction

ORTHOPEDIC implants have become in recent years the standard remedy for the treatment of many diseases of the joints and of the musculoskeletal system including some types of fractures as the ones of long bones (femur, tibia). The most advanced surgical techniques involve the insertion into the medullary canal of special prostheses called "intramedullary nails" [1]. The widespread diffusion of implanted prostheses has given rise to issues of labeling and identification over the years but also to the need of an early detection of pathological phenomena related to the implant itself like local inflammation, infection and rejection. Parameters such as the increase of local temperature, displacement, mechanical stress and abnormal tissue regrowth are precursors of above pathological events and hence a periodic monitoring of the prosthesis health-state [2]–[5] may permit to detect such pathologies in the early stages.

In the emerging scenario of the *Internet of Things* [6], an "augmented" prosthesis will become a wireless-connected sensing node [7], [8] that will be useful to provide live information about the patient thus supporting the post-surgery follow-up and in-home tele-rehabilitation [9]. Due to the long life of a prosthesis, "battery-less" becomes a key requirement so that electronic devices embedded into the prosthesis could wirelessly gather energy through electromagnetic waves for their activation and communication with an external interrogating unit.

Worldwide research about telemetry links with externally powered sensors that are somehow integrated into or over an orthopedic prosthesis mostly concerns low frequency devices with contacting external antennas. One of the first pioneering examples was proposed in 2007 [10]: the implanted sensor harvested energy from the interrogating unit that was equipped with a power supply coil operating at 4 kHz and fixed around the patient. Data about the orthopedic implant load was then transmitted at 150 MHz through a different set of coils. The same authors then described in [11] a possible application of this technology to in-vivo measurement of the local temperature of a hip implant. In [12] an ad-hoc lock-in amplifier was proposed for integration into a remotely-powered sensor to be placed into a hip prosthesis. This telemetry system, operating at 4 kHz and 125 kHz, was aimed at measuring temperature and vibrations of the prosthesis. The antennas of the sensor and of the interrogator were again coils. In [13] a non-radiative transcutaneous link was established at 13.56 MHz by using the Radiofrequency Identification (RFID) protocol in the HF band. In [14] a flexible loop antenna for a bone implant was designed to operate in the 401-406 MHz telemetry band: the communication with the implanted tag required to place external large and uncomfortable coils at direct touch with the body.

Other experiments considered instead the UHF (860-960 MHz) RFID band in case of both contacting and non-contacting interrogators. In particular, a transcutaneous telemetry system, based on the near-field interaction at 915 MHz, was proposed in [15]. A dipole-like tag, equipped with a microchip and a temperature sensor, was directly attached onto the prosthesis. The antenna of the reader was a touch probe, including electrodes, that requires to be placed over the skin, just in front of the implant. A maximum reading depth up to 4cm through pork skin was achieved for 30 dBm power emitted by the contacting antenna of the reader. The potentiality and limitations of UHF-RFID transcutaneous link involving *non-contacting* external exciter/receiver were recently discussed by us in [16] for application to limb implants. The antenna of the reader was a folded patch while the antenna of the sensor was a square loop directly attached onto a bone, by means of a spacer. Simulations with a detailed human model and experiments with phantoms

Manuscript received October 31, 2015; accepted November 15, 2015. Date of publication November 25, 2015; date of current version February 8, 2016. The associate editor coordinating the review of this paper and approving it for publication was Prof. Jun Ohta.

The authors are with the Pervasive Electromagnetic Laboratory, Department of Civil Engineering and Informatics Engineering, University of Roma Tor Vergata, Roma 00133, Italy (e-mail: lodato@disp.uniroma2.it; marrocco@disp.uniroma2.it).

Digital Object Identifier 10.1109/JSEN.2015.2503887

demonstrated that it is feasible to achieve a more than 30 cm link range for tags implanted into shoulder, elbow, hip and knee with 30 dBm of emitted power. We moreover demonstrated that this kind of telemetry is fully compliant with the electromagnetic exposure regulations. However, in spite of the accurate model of the human body, the effect of the prosthesis was only roughly simulated by an aluminum foil enveloping a cow bone without any attempt to address the electromagnetic integration of the tag with a real prosthesis.

The adoption of RFID UHF band for prosthesis interaction deserves specific attention over lower frequency standards (LF and HF) at least for a few attractive advantages. *i*) In spite of the UHF communication is more suffering from the tissue losses than HF links, the interrogation ranges of UHF implants proved to be much longer and suitable to collect the biophysical status of the prosthesis while the patient passes through an electromagnetic gate with a remarkable application to smart-home environments [6]. *ii*) The size of the interrogator of an UHF system is smaller than the HF one so that the antenna could be fabricated with unobtrusive planar technology. This issue is particularly relevant when the reading system has to be wearable for a continuous monitoring of the prosthesis. HF systems as in [11] require uncomfortable coils to get into the limb while UHF reader could have the size of a plaster. *iii*) UHF implanted tags may be naturally used as a permittivity sensor to qualitatively detect changes of tissues close to the prosthesis [17].

Finally a much higher frequency communication link with a prosthesis is described in [18]. A 21 GHz slotted waveguide antenna was conformal to an orthopedic pin suitable to bone lengthening. The antenna exploited the hollow structure of the pin and it was connected to the body surface through a thin dielectric guide in order to harvest energy from an external EM field. After rectification, such energy was used to feed a motor for the control of the lengthening of the pin itself and how to control the electric matching of the microchip impedance.

This paper can be considered the natural evolution of [16] where the effort is now devoted to the investigation on how embedding the functionalities of an UHF tag into a family of real orthopedic prosthesis with minimal modification of their mechanic structure. It is indeed shown how integrating the RFID antenna inside the prosthesis itself. The design approach is borrowed from *structural antenna* technology that was developed years ago for the naval and avionic communication and it is here adapted to produce an ad-hoc UHF Prosthesis Structural Tag carved out of the prosthesis itself, with a rather marginal change.

The paper is organized as follows: Section II introduces the idea of the PST while Section III describes the computer simulations for an intramedullary nail-like PST, aimed at understanding the key geometrical parameters for the frequency tuning of the device. Section IV introduces the prototype of the PST, the experimental phantom and the measurement procedure. The experimental results are finally discussed in Section V also in comparison with simulations in terms of the power required to activate the chip, for two kinds of deep and superficial implants.

	Femoral nail	Tibial nail
Distal diameter (mm)	9-16	8-13
Proximal diameter (mm)	13.5 -16	11-13
Length (mm)	300-480	255-465

Fig. 1. Example of Intramedullary nail and typical dimensions for femur implants and tibial implants.

II. Prosthetic Structural Tag

A transcutaneous link based on the UHF Radiofrequency Identification protocol requires to place a passive transponder, often referred to as *tag,* inside the prosthesis to be monitored. The tag communicates with an external *reader* unit that is composed of a small radar and of an antenna that illuminates the body. The reader energizes the tag from remote through electromagnetic waves and also provides the carrier for the response of the tag. The tag includes a small antenna for energy harvesting and a microchip transponder that switches its internal equivalent RF impedance between two states and accordingly modulates in reflection the impinging carrier so achieving communication by *modulated backscattering*.

The design of the prosthetic tag is based on an antenna architecture that is widely used in naval and aerospace HF (2-30 MHz) communications wherein low-profile radiators are conceived by closely integrating the radiation mechanism into existing metallic super-structures [19] such as the fuselage of an airplane, a funnel or a big mast of a ship, which are used as an active part of the radiating system. The integration of radio-sensing capabilities inside an implanted medical device however demands for additional and more critical constraints. Any change to the original prosthesis has not to compromise its biocompatibility, functionality and its mechanical stability. Moreover, surface discontinuities have to be avoided since they could obstruct the correct insertion of the prosthesis into the bone. The inclusion of radiating elements is therefore required to be low-profile.

Without loss of generality, the idea of a structural RFID tag for bone prosthesis is hereafter described with reference to a specific device, the *intramedullary nail*. The application to a different metallic prosthesis may be considered as straightforward. An intramedullary nail (Fig. 1) consists of an anatomically curved rod generally made of titanium alloy whose size depends on the type of the fracture and on the specific implantation locus such as, for instance, the femur and the tibia. Fixing holes are drilled at the extremities of the device at the purpose to lock the prosthesis to the bone by means of screws. For such kind of prostheses, the feeding part of the antenna could be integrated into one of the fixing hole or within a custom notch carved out of the cylindrical body of the nail without altering the continuity of the external surface and the mechanical strength of the implant.

We recently demonstrated [16] the potentiality of a square-loop RFID tag for insertion in close surrounding of a bone. In particular, the loop layout with its intrinsic inductive reactance, revealed suitable to easily match the capacitive

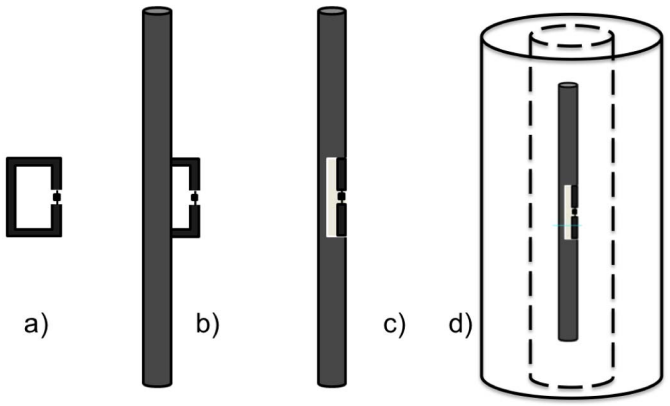

Fig. 2. Integration of a square loop into the body of an intramedullary nail, here simplified by a cylindrical rod. a) Square loop tag; b) towel bar antenna, c) Prosthetic Structural Tag. d) reference geometry of implant inside a cylindrical model of a limb including bone and muscle.

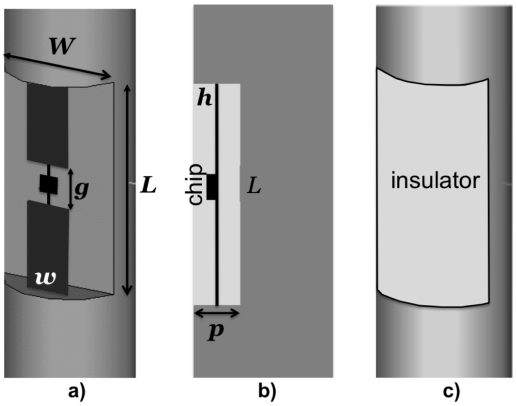

Fig. 3. Details of PST a) the interior of the notch (having removed the dielectric insulator) hosts the two strips where the microchip will be connected; b) side section with indication of the insulator and c) external view.

impedance of the RFID microchip even when the tag was placed in proximity of metallic objects inside a limb phantom. The square loop is now made structural with the nail by following the rationale in Fig. 2. Half the loop can be replaced by the nail itself, like in the *towel-bar antennas* over aircrafts [20]. Further on, at the purpose to avoid protruding elements, the half loop is carved out just inside the cylindrical body. In this way the mechanical continuity and stability of the prosthesis is not altered. The resulting device, hereafter denoted as Prosthetic Structural Tag (PST), resembles a T-match configuration except for the electromagnetic radiation that is mostly produced, as discussed later on, by the embedded half loop, rather than by a true dipole mode.

III. Parametric Analysis and Antenna Design

For the sake of simplicity, the reference prosthesis is hereafter emulated by a straight cylindrical titanium rod of diameter $D = 12$ mm and length $l = 400$ mm that is compliant with the size of conventional Intramedullary nails as in Fig. 1. The excitation section (Fig. 3) comprises a rectangular strip of size $w \times L$ that is suspended inside a notch of size $L \times W \times p$ at a distance h from the external surface. The reference RFID microchip for the numerical simulation is the Impinj Monza-4 (RF impedance $Z_{chip} = 13 - j151\,\Omega$ at 868 MHz and power sensitivity $p_{chip} = -18$ dBmW) that is connected in the middle of the strip. The notch is assumed as filled by an insulating coating having the twofold role to provide isolation from the biological tissue as well as to preserve the external profile of the nail. The rod is finally assumed to be inserted (Fig. 2d) along the axis of a cylindrical bone (diameter 52 mm, permittivity and loss tangent $\epsilon_{bone} = 12.5$, $tan\delta_{bone} = 0.23$) that is in turn placed coaxially into a muscle-equivalent homogeneous cylinder of diameter 140 mm (not shown in the figure) with dielectric parameters $\epsilon_{muscle} = 43$, $tan\delta_{muscle} = 0.25$ simulating a human limb.

The design of the PST consists in optimizing the parameters of the notch and of the excitation strip with the goal to maximize the power that is harvested by the microchip at the European RFID frequency 868 MHz. The performance parameter is accordingly the power transfer coefficient $\tau = 4R_A R_{chip}/|Z_A + Z_{chip}|^2 \leq 1$ at the microchip port, with $Z_A = R_A + jX_A$ being the input impedance seen at the gap of the strip where the microchip is interconnected.

The geometry was modeled by the CST Microwave Studio in order to perform a parametric analysis when the notch sizes changed in the following ranges: $20 \leq L \leq 75$ mm, and $6 \leq W \leq W_x(D, p)$, where the bound $W_x(D, p) = 2\sqrt{(D/2)^2 - (D/2 - p)^2}$ is derived from the intersection between the cylinder and the rod to obtain, by subtraction, the notch region. The remaining parameters were fixed to $p = 4$ mm, $h = p/2$ and $w = 4$ mm. Two values of permittivity $\epsilon_f = \{2, 8\}$ were moreover selected for the filling dielectric that may represent the Teflon and a possible realistic material commonly used in a prosthesis such as ceramics. The Teflon, although not biocompatible, is however considered here since it will be used for the fabrication of a preliminary prototype for laboratory experimentations.

A. Impedance Matching

Fig. 4 shows two matching charts, e.g. the isolines of the power transfer coefficient of the PST for variations of the parameters of the notch. The useful region with $\tau \geq 0.7$ corresponds to the parameters ranges $\{7.5 \leq W \leq 11$ mm, $55 < L < 65$ mm$\}$ and $\{9.5 \leq W \leq 12$ mm, $L = 40$ mm$\}$ for the two cases of low and high permittivity, respectively. As expected, the denser dielectric coating provides a miniaturization of the length of the two strips (size L) but at the price of a smaller tolerance in the size of the notch region (the $\tau \geq 0.7$ area is smaller for this configuration than in the other case).

B. Optimal Configuration

Fig. 5 shows the simulated surface current density at 868MHz for a possible implementation of the PST having $\{W$=8 mm, L=65 mm, p=4 mm, $\epsilon_f = 2\}$ e.g. a small value of the size W of the notch at the purpose to minimize the possible weakening of the mechanical properties of the prosthesis. The surface current density is mostly concentrated into the notch region. The remaining part of the rod is hence nearly isolated by the chocking effect produced by the notch

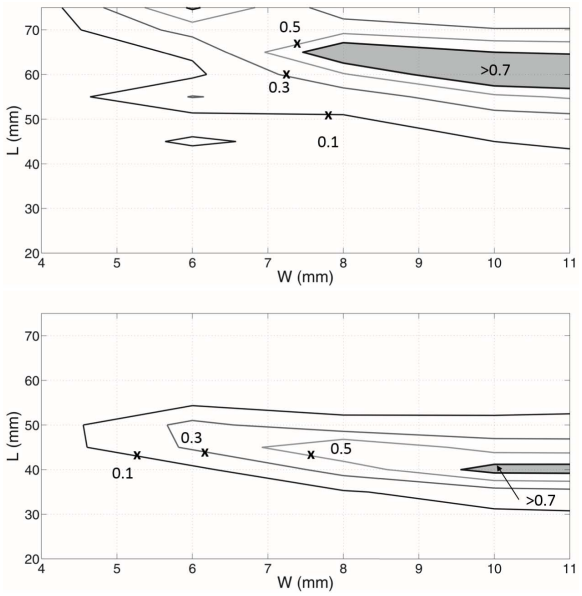

Fig. 4. Isolines of the power transfer coefficients τ as evaluated for two permittivities ϵ_f of the filling dielectric and for a depth of the notch $p = 4$ mm with $W_x(p = 4$ mm $\backsimeq 11$ mm) $W_x(p = 4$ mm Up) $\epsilon_f = 2$ and down) $\epsilon_f = 8$.

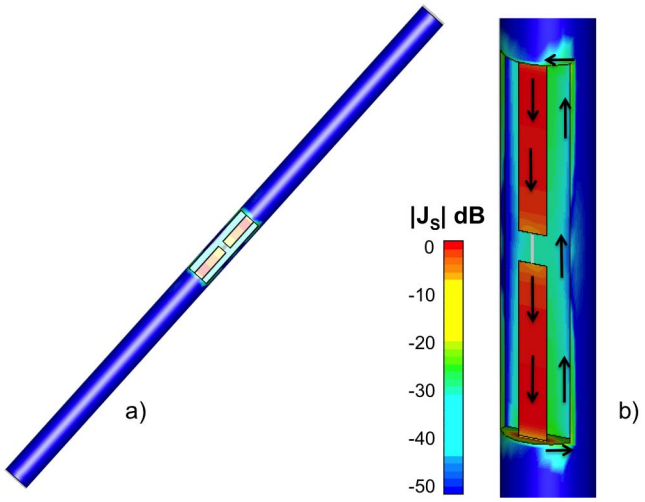

Fig. 5. Normalized simulated current density distribution J_s on a) the whole PST at 868 MHz and b) details of the notch. The color scale is over-expanded at the purpose to highlight the attenuation of the surface current over the rod with respect to the notch region.

plus strips as well as by the presence of the losses of the phantom that yield, in overall, a more than 50 dB attenuation of the surface current with respect to the maximum values occurring on the strips.

Fig. 6 shows the near field of the PST that has been computed by assuming the antenna as in radiating mode. The highest radiation occurs along the cylinder radius just in front of the notch. Although the integration of the chip with the rod visually resembles that of a T-match in conventional RFID sub-wavelength dipoles, the radiation mechanism is completely different. First of all, due to the presence of the body tissues, the effective electrical length of the rod is a few wavelengths and in spite of the concentric arrangement of rod and body-like cylinder, the radiated field is clearly non

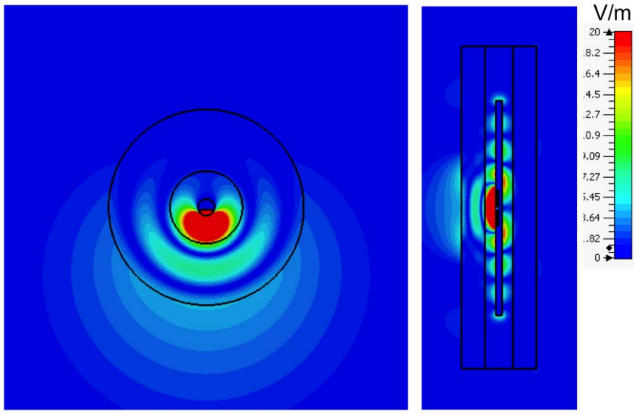

Fig. 6. Simulated electric field radiated by the PST in the nearby region when it is implanted as in configuration of Fig. 2d. a) horizontal cut; b) vertical cut.

isotropic on the horizontal plane unlike the case of dipoles. Moreover the vertical cut in Fig. 6 shows a stationary and quickly attenuating electric field mostly confined inside the bone except for in the proximity of the notch where the radiation occurs.

A deeper understanding of the radiation modality comes out the analysis of input parameters and radiation efficiency of the PST versus frequency and for some lengths of the rod comprising different models of the nail (l={250 mm, 400 mm}) as in Fig. 1 and also an extreme case (l=100 mm) of a very short nail just slightly longer than the notch. Fig. 7 shows only rather marginal variations of all the PST electric parameters and all the considered devices are well matched at the european frequency ($\tau > 0.7$ at 868 MHz). The radiation efficiency is moreover rather stable within a broad range of frequencies so there should be no particular advantage in working above the UHF RFID band.

Finally, the profile of the input impedance has a typical parallel resonance around 1450 MHz with a huge input resistance. Such resonance was verified to be the first one of the PST: the dominant behavior is therefore that of a loop-like structure, rather than of a dipole. The natural inductive reactance at low frequencies is useful to match the RF capacitive impedance of the microchip.

It is therefore reasonable to claim that the electromagnetic performance of the PST is rather stable with respect to the length of the nail and that the PST works as an half loop (towel-bar antenna) embedded into the prosthesis itself. Moreover, only the central part of the prosthesis is electromagnetically active and works as a kind of reflector making the radiation quite directional.

The power transfer coefficient of the optimized geometry of the notch is more than 0.8 at the european UHF frequency for RFID and close to 0.7 in the US band (902-928 MHz).

C. Application to a Realistic Intramedullary Nail Model

To evaluate the applicability of the proposed design methodology to a real intramedullary nail, the more complex geometry in Fig. 1 was finally considered as a starting point. The geometrical and electromagnetic model now includes all the relevant details such as the not uniform profile, the slight

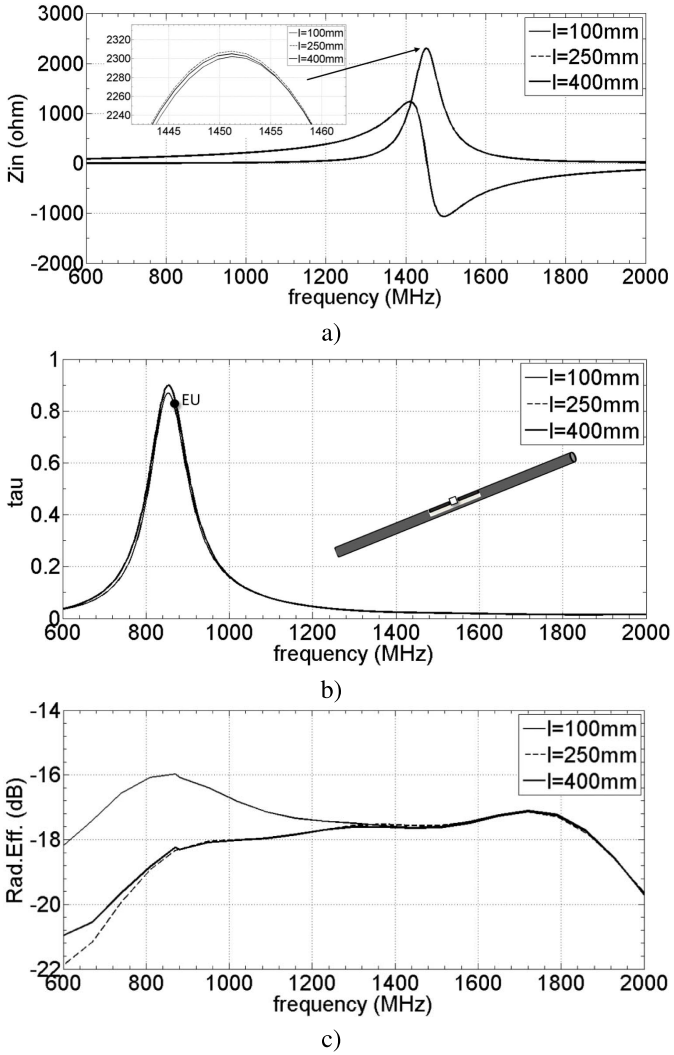

Fig. 7. a) Input impedance of the PST vs. frequency for the case of parameters of the excitation region {W=8 mm, L=65 mm, p=4 mm, $\epsilon_f = 2$}. b) Power transfer coefficient referred to the microchip impedance Z_C. c) Radiation efficiency. Three lengths of the rods have been considered.

bending and the fixing holes (Fig. 8). The conductor is titanium as for the real prosthesis. Since the electromagnetic interaction between the rod and the microchip is rather local, the off-center un-uniformity of the nail is expected to have a negligible impact on the electric response of the overall system. Accordingly, the same matching chart previously derived for the reference cylindrical rod (Fig. 4) was also used to define the notch size for the optimal performance of the intramedullary nail. The choice of geometrical parameters {W=8 mm, L=65 mm, p=4 mm}, permitted to easily achieve a power transfer coefficient (Fig. 8) well tuned in the European UHF RFID band.

IV. Prototype, Phantoms and Measurement Procedure

A. PST Prototype

A prototype of the simplified PST was fabricated by using a cylindrical steel rod (Fig. 9) of total length $l = 290$ mm and diameter $D = 12$ mm. The notch was centrally carved in

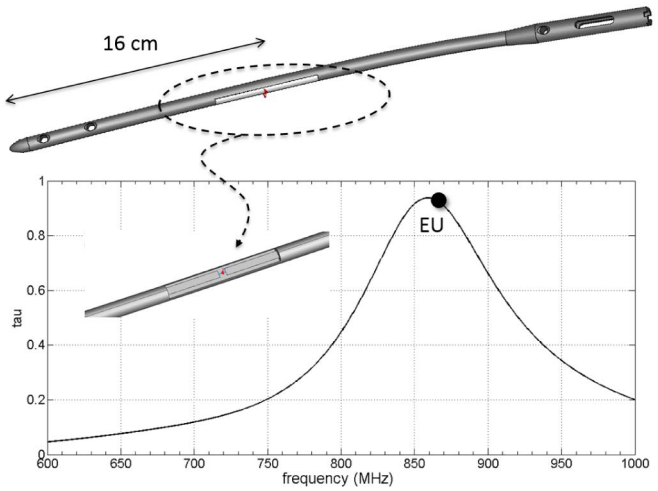

Fig. 8. (Up) Transformation of a real intramedullary nail into a structural tag. (Down) Simulated power transmission coefficient and detail of the radiating notch. Size of the notch and exciter: {W=8 mm, L=65 mm, p=4 mm}.

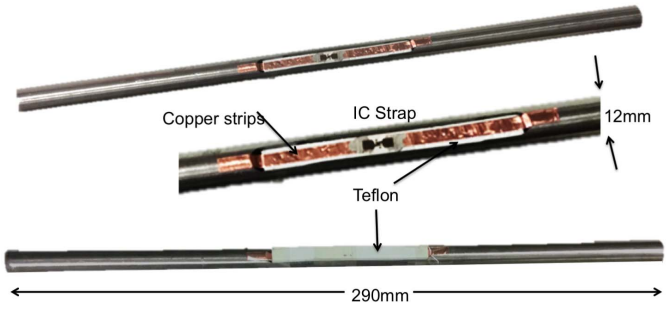

Fig. 9. Steel prototype of PST resembling an intra-medullary nail that is here shown, for clarity, without and with the external insulating Teflon layer.

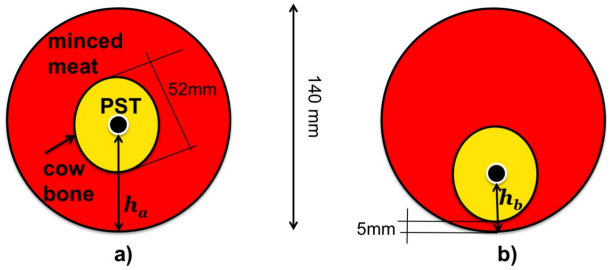

Fig. 10. Detailed geometry of the phantoms of the limb for laboratory experimentations. A glass cylinder was homogeneously filled with minced meat and the PST prototype was inserted inside the medullary canal of a cow bone that was in turn placed at two different distances from the glass at the purpose to emulate a) a femoral nail ($h_a = 70$ mm) and b) a more superficial implant as a tibial nail ($h_b = 25$ mm).

the rod and had sizes $W = 8$ mm, $L = 65$ mm, $p = 4$ mm, according to the previously simulated model.

The interconnection of the microchip to the rod was achieved by means of two metal copper strips (width 4 mm). The inner and external dielectric coatings consist of two sheets of Teflon having 2 mm thickness (Fig. 9). This prototype can be considered as representative of both a tibial and a femoral nail.

B. Limb Phantom

The limb phantom (Fig. 10) was assembled by a glass cylindrical pipe, of diameter 140 mm filled with minced meat

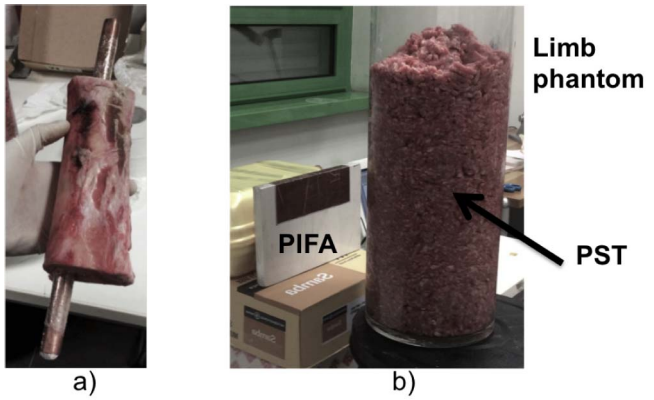

Fig. 11. a) PST placed inside the medullary canal of a cow bone and b) the measurement set-up comprising the limb phantom with the bone inside and a ThingMagic M5 reader (not shown) connected to a Stacked PIFA antenna.

(moisture of muscle with 35% of fat) up to a height of 350 mm. The PST was implanted inside the medullary canal (Fig. 11d) of a cow bone (average diameter 52 mm and bone-thickness 20 mm) placed at two different distances from the lateral surface of the box. A first configuration (Fig. 10a) with $h_a = 70$ mm emulates a deep (femoral) implant, while in a second configuration (Fig. 10b) the bone was placed at a closer distance from the pipe surface ($h_b = 25$ mm) at the purpose to simulate a more superficial (tibial) implant.

C. Measurement Setup

The measurement setup (Fig. 11) comprised a ThingMagic M5e reader connected to a broadband linear polarized Stacked Planar Inverted-F Antenna (S-PIFA) that includes a teflon substrate with external size $13x20$ cm^2 and exhibits a maximum gain of 5.5 dBi along its normal axis.

D. Measurement Procedure

The performance parameters of the RFID link are the *turn-on power* P_{to} and the *Direct Link Margin* M_{DL}. The turn-on power is the minimum power emitted by the reader that is required to activate the tag in the specific configuration. The upper bound of P_{to} is the maximum power that the reader may provide the interrogating antenna with. The direct-link margin (in dB) is defined [16] as:

$$M_{DL} = P_{R\to T}|_{dB} - p_{chip}|_{dB} \tag{1}$$

where

$$P_{R\to T} = G_T P_{av} \tag{2}$$

is the power delivered by the reader to the IC when the reader emits the maximum available power P_{av} (here 30 dBmW with the available hardware) and G_T is the transducer power gain [21]. The condition $M_{DL} > 0$ ensures that the power emitted by the reader is enough to activate the chip and hence to establish a correct RFID communication. Even for the case of implanted tags, the direct link was previously demonstrated to be still the bottleneck [16] of the communication and hence the check on the above margin is sufficient

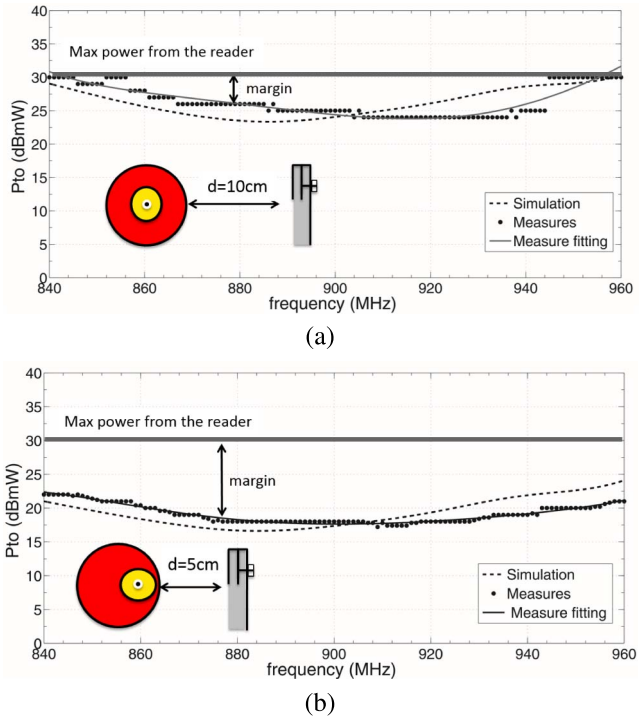

Fig. 12. Simulated and measured turn-on power P_{to} for PST implanted as in Fig. 10 having included also the S-PIFA antenna of the reader that is placed at distances d={10 cm, 5 cm}, respectively.

to assess the feasibility of the link. The higher the direct margin is, the more the chip of the tag will harvest power in excess that could be useful to energize additional onboard sensors.

During the measurement, the power emitted by the reader was increased until the chip was activated, thus obtaining the turn-on power. The transducer gain is accordingly determined as:

$$G_T = \frac{p_{chip}}{P_{to}} \tag{3}$$

The direct-link margin can be hence finally derived throughout (2), (1) and (3) as

$$M_{DL} = P_{av}|_{dB} - P_{to}|_{dB}. \tag{4}$$

V. Results

Reference data for comparison with measurements were moreover obtained by means of numeric simulations which accounted for the whole RFID link. At the purpose to correctly predict the electromagnetic coupling between the various devices without any far-field assumption, simulations included the limb phantom, the cow bone (as in Fig. 10) and both the PST and the antenna of the reader as well.

The values of the simulated and measured turn-on powers (Fig. 12) show that the RFID communication was correctly established even in the most challenging case of the deeper implant in the center of the phantom with the reader placed at the larger distance $d = 10$ cm. The direct link margin was $M_{DL} = 4$ dB in the European RFID band and up 6 dB in the US band (902-928 MHz). The margin was even better

TABLE I

MEASURED TRANSDUCER POWER GAIN G_T A THE EUROPEAN AND US FREQUENCIES FOR THE TWO KINDS OF IMPLANT

Configuration	868 MHZ	910 MHZ
femoral nail (Fig.10a)	−40 dB	−38 dB
tibial nail (Fig.10b)	−33 dB	−32 dB

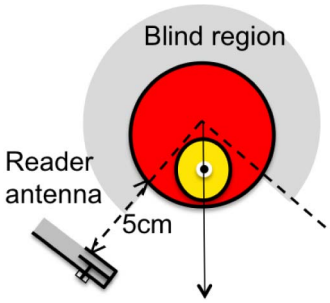

(°)	GT (dB)	Pto (dBm)
0	-37.5	20
45	-37.5	20
90	<-47.5	>30
180	<-47.5	>30
-90	<-47.5	>30
-45	-37.5	20

Fig. 13. Measured transducer power gain and turn-on power around the phantom simulating a tibial implant for an average reader-tag distance of 5cm. The shadowed circular sector indicates the angular region where the reader was unable to detect the smart prosthesis.

TABLE II

EXPERIMENTAL MAXIMUM READ RANGES FOR THE TWO TYPES OF IMPLANT AT 868 MHz WHEN THE READER PROVIDE ITS ANTENNA WITH 1 W INPUT POWER

Implant type	maximum read distance
femoral nail (Fig.10a)	23 cm
tibial nail (Fig.10b)	45 cm

($M_{DL} = 14$ dB in both EU and US bands) for the rod implanted close to the skin and by using a closer ($d = 5$ cm) interrogator. In both cases, measurements are in reasonable agreement with simulations, even if a mutual frequency shift is apparent and is probably due to the approximate knowledge of the real parameters of the used biologic materials and on the imperfection in the manual fabrication of the prototype.

The transducer power gains for the two configurations evaluated at the European and US frequencies are shown in Tab.I. The values are of the same order (−40 to −30 dB) of those found in [16] for a square loop tag that was simply placed on the lateral surface of a cow bone enveloped by an aluminum sheet.

In a second experimental session, the angular dependency of the RFID link was evaluated by moving the antenna of the reader around the phantom at a fixed 5 cm distance from its surface, when the PST was still implanted as shown in Fig. 10b). The resulting angular read region (Fig. 13) was centered around the notch $\{-45° \leq \varphi \leq 45°)$ while the prosthesis was fully unreachable when interrogated from the lateral and rear sides. This result is in agreement with the simulated near field plot of Fig. 6.

We finally evaluated the maximum reading distances from the cylinder surface to the PIFA antenna (Tab.II) for both the two considered configurations. The reader emitted a fixed 30 dBmW power at 868 MHz and the interrogating antenna was hence moved away from the phantom until the chip stopped responding. In both the cases such distances could permit a comfortable interrogation by an hand-held antenna which an operator moves around the limb. In the more favorable case of tibial nail, the larger distance could be even compatible with an automatic reading through a gate-like set-up when the user is moving for instance inside his domestic environment.

VI. CONCLUSION

The main achievement of this paper is the demonstration that a prosthetic with cylindrical body may be hacked with minimal mechanical changes to obtain transcutaneous communication capability with an external UHF-RFID interrogating module up to a distance of some tents of centimeters. The strong power absorption of the human tissues makes the radiation mechanism rather local so that more than a single notch could in principle be integrated into a same long prosthesis, so enabling a few spatial diversity in the monitoring of the prosthesis status.

As discussed in [16], the interrogation of the tag inside the prosthesis by external electromagnetic waves can be considered fully compliant with the exposure standards. In particular, by assuming the extreme case of a reader's antenna (a PIFA) placed at 5cm from the skin and continuously (duty cycle=1) radiating 3.2 W EIRP (the maximum power allowed in Europe,) the estimated Specific Absorption Rate (SAR) weighted on 10 g (as required by standards) was SAR(10)<0.25 W/Kg that is only a small fraction of the maximum allowed level (SAR<4 W/Kg).

The achieved results encourage the experimentation with the new-generation of sensor-oriented RFID microchips for the direct measurement of mechanical stress and of the local temperature with great potentiality of detection of early inflammatory or stressful events.

ACKNOWLEDGMENT

The authors wish to thank prof. P. P. Valentini for valuable discussions and technical support concerning the mechanical sustainability of the PST concept.

REFERENCES

[1] G. W. Wood, II, "Intramedullary nailing of femoral and tibial shaft fractures," *J. Orthopaedic Sci.*, vol. 11, no. 6, pp. 657–669, 2006.
[2] W. Xu, "Instrumentation and experiment design for in-vitro interface temperature measurement during the insertion of an orthopaedic implant," in *Proc. 10th Int. Conf. Control, Autom., Robot. Vis. ICARCV)*, Dec. 2008, pp. 1773–1778.
[3] J. F. Drazan *et al.*, "Archimedean spiral pairs with no electrical connections as a passive wireless implantable sensor," *J. Biomed. Technol. Res.* vol. 1, no. 1, pp. 1–8, 2014.
[4] H. Chen *et al.*, "Low-power circuits for the bidirectional wireless monitoring system of the orthopedic implants," *IEEE Trans. Biomed. Circuits Syst.*, vol. 3, no. 6, pp. 437–443, Dec. 2009.
[5] F. Burny *et al.*, "Concept, design and fabrication of smart orthopedic implants," *Med. Eng. Phys.*, vol. 22, no. 7, pp. 469–479, 2000.
[6] S. Amendola, R. Lodato, S. Manzari, C. Occhiuzzi, and G. Marrocco, "RFID technology for IoT-based personal healthcare in smart spaces," *IEEE J. Internet Things*, vol. 1, no. 2, pp. 144–152, Apr. 2014.
[7] E. Ghafar-Zadeh, "Wireless integrated biosensors for point-of-care diagnostic applications," *Sensors*, vol. 15, no. 2, pp. 3236–3261, 2015.

[8] R. C. Wasielewski, "Wireless technologies for the orthopaedics: Diagnostics and surgical applications," in *Proc. IEEE Topical Conf. Biomed. Wireless Technol., Netw., Sens. Syst. (BioWireleSS)*, Jan. 2011, pp. 1–2.
[9] M. Hamel, R. Fontaine, and P. Boissy, "In-home telerehabilitation for geriatric patients," *IEEE Eng. Med. Biol. Mag.*, vol. 27, no. 4, pp. 29–37, Jul./Aug. 2008.
[10] F. Graichen, R. Arnold, A. Rohlmann, and G. Bergmann, "Implantable 9-channel telemetry system for in vivo load measurements with orthopedic implants," *IEEE Trans. Biomed. Eng.*, vol. 54, no. 2, pp. 253–261, Feb. 2007.
[11] G. Bergmann, F. Graichen, J. Dymke, A. Rohlmann, G. N. Duda, and P. Damm, "High-tech hip implant for wireless temperature measurements in vivo," *PLoS One*, vol. 7, no. 8, pp. 1–7, 2012.
[12] U. Marschner *et al.*, "Integration of a wireless lock-in measurement of hip prosthesis vibrations for loosening detection" *Sens. Actuators A, Phys.*, vol. 156, no. 1, pp. 145–154, 2009.
[13] X. Liu, J. L. Berger, A. Ogirala, and M. H. Mickle, "A touch probe method of operating an implantable RFID tag for orthopedic implant identification," *IEEE Trans. Biomed. Circuits Syst.*, vol. 7, no. 3, pp. 236–242, Jun. 2013.
[14] R. Alrawashdeh, Y. Huang, and A. A. B. Sajak, "A flexible loop antenna for biomedical bone implants," in *Proc. 8th Eur. Conf. Antennas Propag. (EuCAP)*, Apr. 2014, pp. 861–864.
[15] X. Liu, J. R. Stachel, E. Stachel, M. H. Mickle, and J. L. Berger, "The UHF Gen 2 RFID system for transcutaenous operation for orthopedic implants," in *Proc. IEEE Int. Instrum. Meas. Technol. Conf. (I2MTC)*, May 2013, pp. 1620–1623.
[16] R. Lodato, V. Lopresto, R. Pinto, and G. Marrocco, "Numerical and experimental characterization of through-the-body UHF-RFID links for passive tags implanted into human limbs," *IEEE Trans. Antennas Propag.*, vol. 62, no. 10, pp. 5298–5306, Oct. 2014.
[17] C. Occhiuzzi, G. Contri, and G. Marrocco, "Design of implanted RFID tags for passive sensing of human body: The STENTag," *IEEE Trans. Antennas Propag.*, vol. 60, no. 7, pp. 3146–3154, Jul. 2012.
[18] P. Zakavi, N. C. Karmakar, and I. Griggs, "Wireless orthopedic pin for bone healing and growth: Antenna development," *IEEE Trans. Antennas Propag.*, vol. 58, no. 12, pp. 4069–4074, Dec. 2010.
[19] G. Marrocco and L. Mattioni, "Naval structural antenna systems for broadband HF communications," *IEEE Trans. Antennas Propag.*, vol. 54, no. 4, pp. 1065–1073, Apr. 2006.
[20] G. Marrocco and P. Tognolatti, "New method for modelling and design of multiconductor airborne antennas," *IEE Proc. Microw. Antennas Propag.*, vol. 151, no. 3, pp. 181–186, Mar. 2004.
[21] S. J. Orfanidis. "Electromagnetics waves and antennas." [Online]. Available: http://www.ece.rutgers.edu/~orfanidi/ewa, accessed Mar. 1, 2015.

Rossella Lodato was born in Palermo, Italy, in 1968. She received the Laurea degree in electronics engineering from the University of Palermo, Palermo, in 2000. From 2007 to 2011, she was a Research Fellow with the Technical Unit of Radiation Biology and Human Health, Italian National Agency for New Technologies, Energy and Sustainable Economic Development, where her research activity regarded the realization and the dosimetry of exposure systems for *in vivo* and *in vitro* experiments for the study of the biological effects of electromagnetic fields. She is currently a Doctorate Fellow of Geoinformation with the University of Rome Tor Vergata, Rome, Italy, on a project concerning implantable RFID systems for biological parameters monitoring.

Gaetano Marrocco received the Laurea degree in electronics engineering and the Ph.D. degree in applied electromagnetics from the University of L'Aquila, Italy, in 1994 and 1998, respectively. In 1994, he was at the University of Illinois at Urbana–Champaign as a Post-Graduate Student. In 1997, he joined the University of Roma Tor Vergata, Italy, as a Researcher. In 1999, he was a Visiting Researcher at the Imperial College, London, U.K. In 2015, he was a Guest Professor at the University of Paris-est Marne la Vallèe. He currently serves as an Associate Professor of Electromagnetics at the University of Roma Tor Vergata, and chairs the Pervasive Electromagnetics Laboratory. His research is mainly focused on the application of radiofrequency identification to medical and industrial diagnostics as well as to the modeling and design of distributed and miniaturized conformal antenna clusters over ships, micro- and nano-satellites and aircrafts within the framework of the European Space Agency, NATO, the Italian Space Agency, and the Italian Navy research projects. In the past, he was moreover active in the development of FDTD methods for microwave hyperthermia and in the modeling and design of pulsed arrays. In 2014, he received the Full Professorship Qualification. He served as an Associate Editor of the IEEE ANTENNAS AND WIRELESS PROPAGATION LETTERS, a Contributor of the IEEE RFID VIRTUAL JOURNAL, and as the Vice Chair of the Italian Delegation URSI Commission D: Electronics and Photonics. He was the Chair of the Local Committee of EUCAP-2011 in Roma and the TPC Chair of the 2012 IEEE-RFID TA, Nice, France. He is the Co-Founder and President of the University spin-off RADIO6ENSE, which is active in the short-range electromagnetic sensing for Industry, Internet of Things, and Smart Cities.